Cheng, Yi; Yu, Wentao; Xie, Jin; Wang, Ruoyu; Cui, Guang; Cheng, Xu; Li, Mengwen; Wang, Kun; Li, Junliang; Sun, Zhipei; Chen, Ke; Liu, Kaihui; Liu, Zhongfan

Controllable Growth of Graphene Photonic Crystal Fibers with Tunable Optical Nonlinearity

Published in:
ACS Photonics

DOI:
10.1021/acsphotonics.1c01823

Published: 01/01/2021

Document Version
Peer-reviewed accepted author manuscript, also known as Final accepted manuscript or Post-print

Please cite the original version:
Cheng, Y., Yu, W., Xie, J., Wang, R., Cui, G., Cheng, X., Li, M., Wang, K., Li, J., Sun, Z., Chen, K., Liu, K., & Liu, Z. (2021). Controllable Growth of Graphene Photonic Crystal Fibers with Tunable Optical Nonlinearity. *ACS Photonics*, *9*(3), 961–968. https://doi.org/10.1021/acsphotonics.1c01823

Controllable Growth of Graphene Photonic Crystal Fibers with Tunable Optical Nonlinearity

Yi Cheng, Wentao Yu, Jin Xie, Ruoyu Wang, Guang Cui, Xu Cheng, Mengwen Li, Kun Wang, Junliang Li, Zhipei Sun, Yue Qi, Ke Chen,* Kaihui Liu,* and Zhongfan Liu**

Y. Cheng, R. Y. Wang, Dr. G. Cui, K. Wang, Dr. Y. Qi, Prof. Z. F. Liu
Center for Nanochemistry, College of Chemistry and Molecular Engineering, Peking University, Beijing 100871, China
E-mail: zfliu@pku.edu.cn; qiyue-cnc@pku.edu.cn

Dr. W. T. Yu, J. Xie, X. Cheng, Prof. K. H. Liu
State Key Laboratory for Mesoscopic Physics, Frontiers Science Center for Nano-optoelectronics, School of Physics Peking University, Beijing 100871, China
E-mail: khliu@pku.edu.cn

Prof. K. Chen
Center for the Physics of Low-Dimensional Materials, School of Physics and Electronics, Henan University, Kaifeng 475004, China
E-mail: kchen@henu.edu.cn

J. Xie, Prof. K.H. Liu
Academy for Advanced Interdisciplinary Studies, Collaborative Innovation Center of Quantum Matter, Peking University, Beijing 100871, China

M. W. Li, J. L. Li, Dr. Y. Qi, Prof. K. Chen, Prof. K. H. Liu and Prof. Z. F. Liu
Beijing Graphene Institute (BGI), Beijing, 100095, China

Prof. Z. P. Sun
Department of Electronics and Nanoengineering, Aalto University, Espoo 02150, Finland

Keywords: graphene, photonic crystal fiber, pressure-controllable chemical vapor deposition, nonlinear harmonic generation, all-fiber laser

Graphene optical fiber, with the merits of high optical nonlinear susceptibility and long light-matter interaction length, has shown enormous potential in all-fiber optical nonlinear applications. In recent works, chemical vapor deposition (CVD) has been proven to be an effective approach to synthesize graphene optical fiber with high quality and massive manufacturing capacity. However, for nonlinear applications, it is extremely significant for the tradeoff between the nonlinear light-matter interaction strength and the undesirable linear absorption loss of graphene. Here, we propose a pressure-controllable CVD strategy for the precise control of the uniform fiber length and graphene thickness, realizing the strong nonlinear effect of graphene photonic crystal fiber (Gr-PCF) with the acceptable loss. Based on the as-fabricated Gr-PCF, the third and fifth harmonic signals exhibit nearly one order of magnitude enhancement compared with those of graphene on planar quartz. In addition, an ultrafast all-fiber laser based on Gr-PCF as a saturable absorber is demonstrated with ~8 mW output power, ~2 ps pulse width and ~37 MHz repetition frequency. Our results technically open up an infusive way to precisely engineer the optical properties of Gr-PCF and broaden its applications in all-fiber photonic and optoelectronic devices.

Optical fiber, with high-quality waveguide capacity and structure designability, has shown its superiority in photon manipulation and optical communication during the past decades.[1-4] Therein, the nonlinear optics in fiber boosts vast attractions for all-fiber nonlinear applications, such as frequency conversion, supercontinuum generation, and mode-locked fiber laser.[5-9] To date, many efforts have been devoted to enhance the nonlinearity of optical fiber, which can be mainly divided into two routes: (i) selectively injecting or filling nonlinear elements/materials into fiber, such as chalcogenide, bismuth oxide and semiconductors, however, still limited in weak nonlinear interaction;[10-12] (ii) designing artificial fiber structures, such as the nonlinear photonic crystal fiber (PCF), whereas faces dilemma of poor function-designing flexibility.[13-15] Naturally, conventional optical materials with high nonlinear susceptibility are of great expectation to be integrated with optical fiber. However, there is currently no available technique that can directly grow these bulk crystals into fiber without severely disturbing their propagation modes. Hence, the emergence of atomic-thick graphene provides a feasible alternative and endows traditional optical fiber with intriguing optical nonlinear properties and intact propagation capacity.[16-19]

Recently, graphene has been integrated with optical fiber by injecting graphene dispersion into the holes of fiber,[20,21] spinning graphene flakes or transferring graphene films on D-shaped or tapered fiber.[22-24] However, these graphene optical fibers are constrained with the short light-matter interaction length, the distortion in the waveguide capacity and the low production efficiency.[20-23] In our previous work, half-meter long graphene-PCF (Gr-PCF) was successfully synthesized with a high-quality graphene film deposited on the inner walls of PCF hole through low pressure chemical vapor deposition (LPCVD) growth method.[18] Nevertheless, for nonlinear applications of Gr-PCF, it is in great demand to realize the balance between the nonlinear light-matter interaction and the undesirable broadband linear absorption loss of graphene, which can be manipulated by the graphene thickness and the fiber length. When the graphene thickness and fiber length increase, nonlinear light-matter interaction of Gr-

PCF increases with the simultaneous increase of the linear absorption loss, leading to the saturable or even decreased behavior of the nonlinear signal. Unfortunately, the precise manipulation of graphene thickness and fiber length has not been achieved yet, considering the challenges of gas flow control inside the micrometer-sized fiber holes.

As a key parameter for graphene growth, system pressure can influence the mean free path and fluid state of the reactant molecules inside the microholes. As system pressure increases, the mean free path of the flowing gas decreases with the gradual increase of the molecular collisions in the gaseous phase and the decrease of gas flow velocity, leading to the decrease of the uniform fiber length along fiber axis. Meanwhile, the concentration of active carbon species also increases, resulting in an increase of graphene thickness.[25-30] Here, we propose a pressure-controllable CVD (PCCVD) strategy to precisely control the uniform fiber length and graphene thickness, and thus achieve the strong nonlinear effect of Gr-PCF with acceptable linear absorption.

In our experiment, Gr-PCF with a solid core and regular arranged air holes of ~2.6 μm (**Figure 1**a) was manufactured by using methane precursor under the growth temperature of 1100 °C. The growth of graphene film inside PCF was directly evinced by the darker contrast of Gr-PCF (Figure 1b, upper panel), compared with the bare PCF (Figure 1b, lower panel). Meanwhile, the intact structure of the as-fabricated Gr-PCF was maintained after the growth, confirmed by the cross-section scanning electron microscopy (SEM) image (Figure S1, Supporting Information). Furthermore, the collapsed graphene tubes were obtained after etching the fiber silica and demonstrated the full coverage of graphene inside the PCF holes (Figure S2 and S3, Supporting Information). The high-resolution transmission electron microscopy (HR-TEM) image (Figure 1c) exhibited the regularly arranged crystalline structure with regular Moiré patterns, confirming the high crystallinity of as-fabricated graphene films.

To clarify the influence of pressure during graphene growth, the pressure-controllable experiments were carried out in the Gr-PCF synthesis. With the increase of growth pressure,

the nonuniformity along the fiber axis became much severer (Figure 1d,e). In order to evaluate the uniformity of Gr-PCF, the uniform length of Gr-PCF was defined by Raman characterization, where the variations of the intensity ratio of 2D- to G-mode Raman peak (I_{2D}/I_G) and full width at half maximum of 2D-mode peak ($FWHM_{2D}$) are supposed to be less than 10%.[18,31] As system pressure increased from 1 to 20 Torr, the uniform length of Gr-PCF significantly decreased from ~50 cm to ~11 cm (Figure 1f and Figure S4, Supporting Information). Besides, we specifically manipulated the graphene thickness under pressure ranging from 1 to 2 Torr. The slight variations of I_D/I_G (the intensity ratio of D- to G-mode Raman peak) and I_{2D}/I_G in Raman spectra (Figure S5, Supporting Information) along the fiber axis demonstrated the high uniformity of as-fabricated Gr-PCF within the uniform length. AFM characterizations revealed that the thickness of the etched graphene tube can be uniformly tuned from ~2.0 to ~3.4 nm with the variations of growth pressure in this range (Figure 1g,h). The corresponding graphene layer number increased from quasi-monolayer to 4-5 layers by TEM characterizations (Figure S6, Supporting Information). When the growth pressure further increases to 20 Torr, the thickness of the graphene tubes can thereby increase to ~17.4 nm (Figure 1i and Figure S7, Supporting Information).

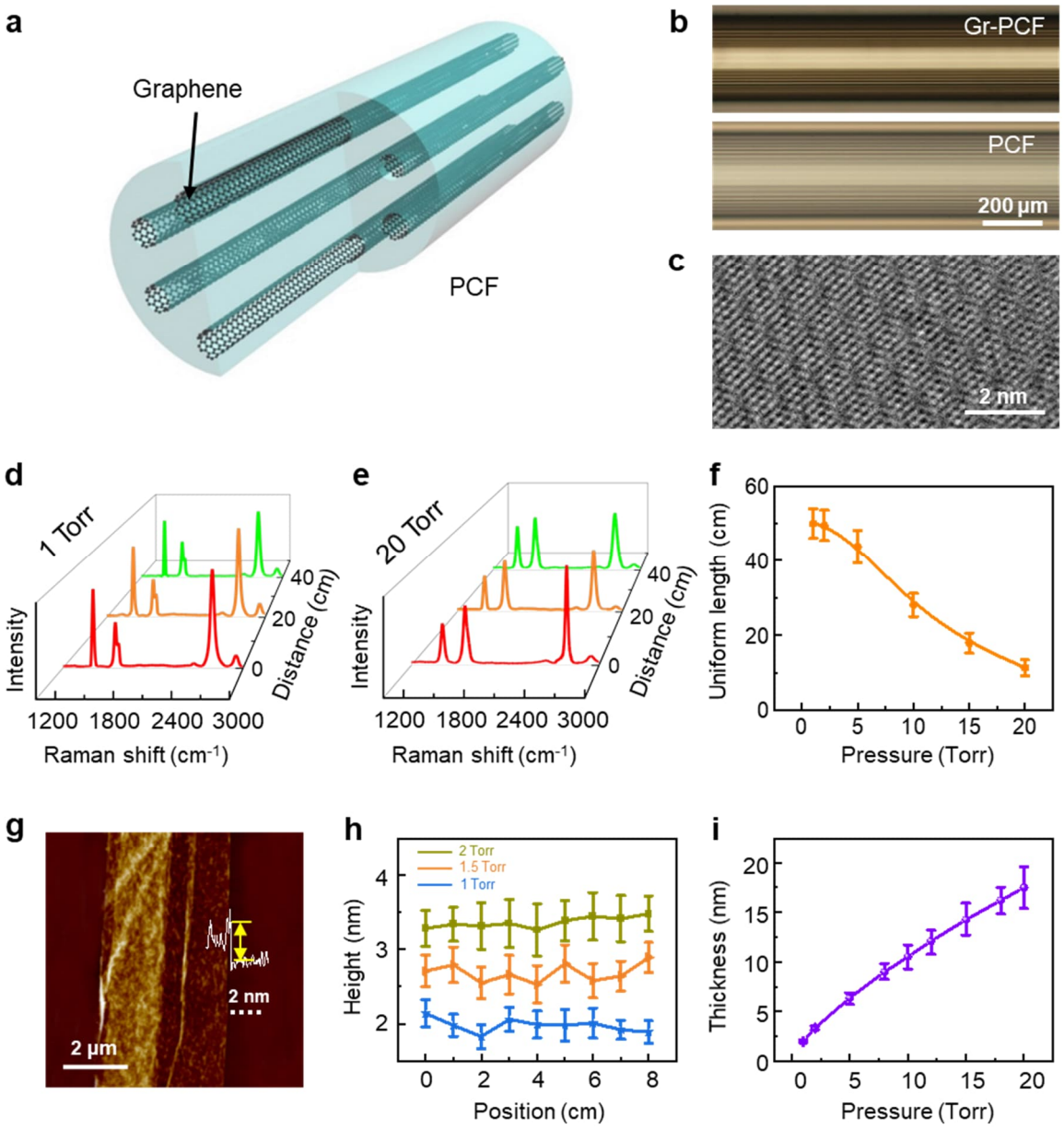

Figure 1. Synthesis of Gr-PCF by PCCVD method. a) Schematic of Gr-PCF structure. b) Optical image of the Gr-PCF (upper panel) and bare PCF (lower panel). c) HRTEM image of the collapsed graphene tube after etching the fiber silica. d,e) Raman spectra of graphene at different positions (with a distance of 20 cm) of collapsed graphene tube along the gas flow under the growth pressure of 1 Torr (d) and 20 Torr (e). f) The variation of uniform fiber length with respect to the growth pressure. g) AFM image of the collapsed graphene tube. h) The thickness of graphene tubes along the fiber axis under different growth pressures. The blue star, orange triangle and dark yellow square represent the fiber sample synthesizing under 1 Torr, 1.5 Torr and 2 Torr, respectively. i) Average thickness of the graphene changing with the increase of the growth pressure.

The graphene growth atmosphere was further investigated by the fluid simulation and the graphene growth behaviors were schematically presented in **Figure 2**a. With the growth pressure changing from 1 to 20 Torr, the fluid state of the reactant gas would transform from the free molecular flow to viscous-molecular transition state (Supporting Information, Note 1), leading to the decrease of the mean free path of the reactant molecular and the gas velocity in the fiber hole (Figure 2b,c), which gave rise to the thus-shortened uniform fiber length (Figure S8, Supporting Information).[18,32] Besides, the concentration distributions of the carbon precursors in the microholes significant increases along the central fiber axis from ~0.01 to ~0.21 mol/m^3 with the growth pressure increase from 1 to 20 Torr (Figure 2d,e), resulting in the increase of graphene thickness. In brief, the PCCVD strategy can facilitate the precise manipulation of the uniform fiber length and graphene thickness for the fine integration of graphene and PCF.

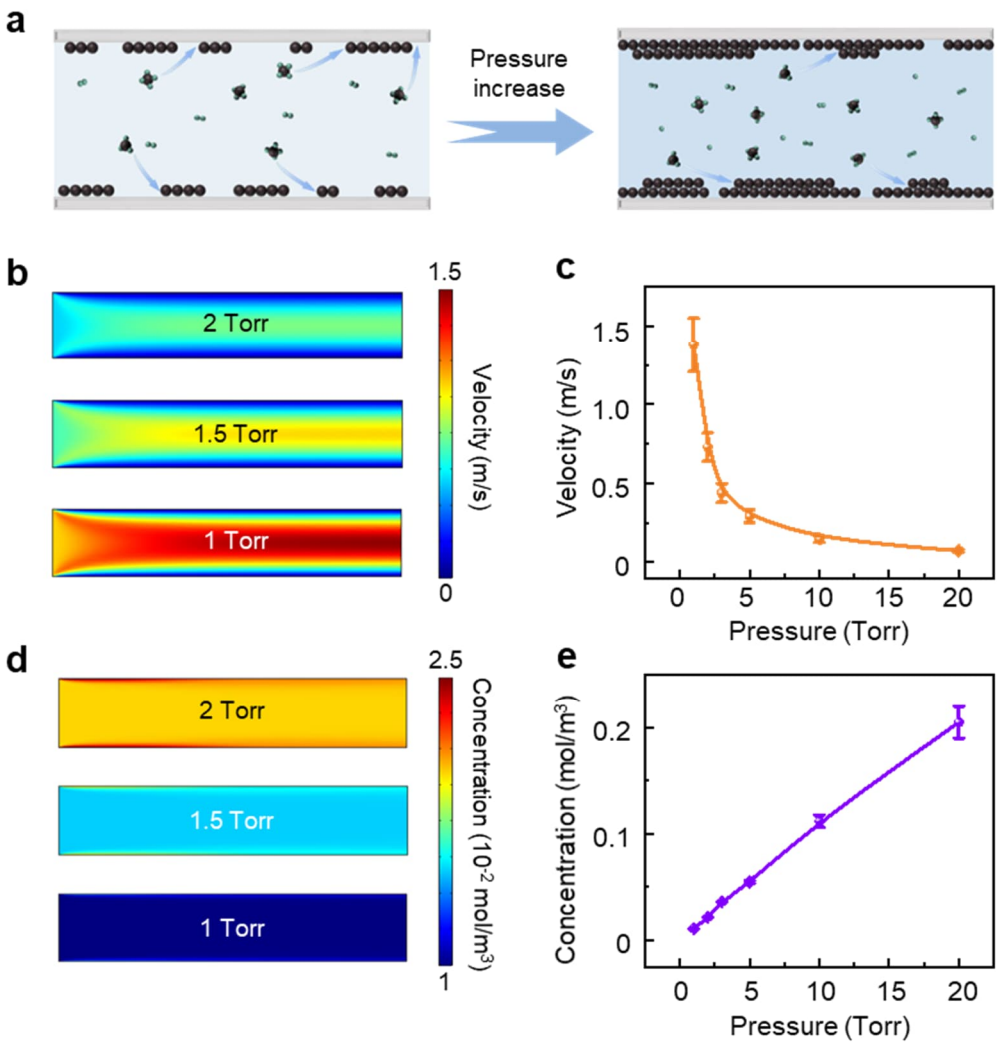

Figure 2. Fluid simulations in the PCF holes. a) Schematic of graphene growth inside the holes of PCFs with the increase of growth pressure. b,c) 2D simulated distributions of the gas flow velocity (b) and the calculated average gas flow velocity (c) along the central fiber axis with respect to the growth pressure. d,e) Corresponding simulated methane concentration distributions (d) and its concentration (e) under different growth pressures.

On the basis of the perfect integration capacity, the Gr-PCF can maintain the intact light waveguide mode and exhibit strong light-matter interaction, which has demonstrated various potential applications in nonlinear optics. Generally, optical nonlinear applications include the following two parts: (i) nonlinear frequency conversion related to the real part of nonlinear susceptibility, such as nonlinear harmonic generation, parametric process and supercontinuum generation, and (ii) nonlinear absorption related to the imaginary part, such as saturable absorption and related mode-locked pulse generation. By using as-fabricated Gr-PCF, we

synchronously yield the applications in nonlinear harmonic generation and all-fiber mode-locked laser, providing the potential development direction of Gr-PCF.

As a representative nonlinear application related to the real part of optical nonlinear susceptibility, the nonlinear harmonic generation, such as third and fifth harmonic, was utilized to clarify the excellent optical nonlinearity of Gr-PCF (**Figure 3**a). Considering the high nonlinear susceptibility of the monolayer graphene and the trade-off between the strong nonlinear light-matter interaction and the inevitable linear absorption loss, the Gr-PCF with monolayer graphene and suitable fiber length was desirable for the nonlinear harmonic generation. Therefore, the 5-cm-long Gr-PCF with quasi-monolayer graphene film demonstrated 10-fold enhancement for third and 6-fold enhancement for fifth harmonic signal, compared with those of graphene grown on planar quartz (Figure 3b). The nonlinear signals monotonically increased with the fiber length shorter than 5 cm, and then decreased with a further elongation of fiber length (Figure 3c). It may be attributed to the gradually increased absorption loss of both incident and nonlinear harmonic light with the increase of fiber length. Meanwhile, a near cubic/fifth dependence of the third/fifth harmonic signal intensity to excitation power was observed as expected in Gr-PCF (Figure 3d), consistent with the theoretical expectation.

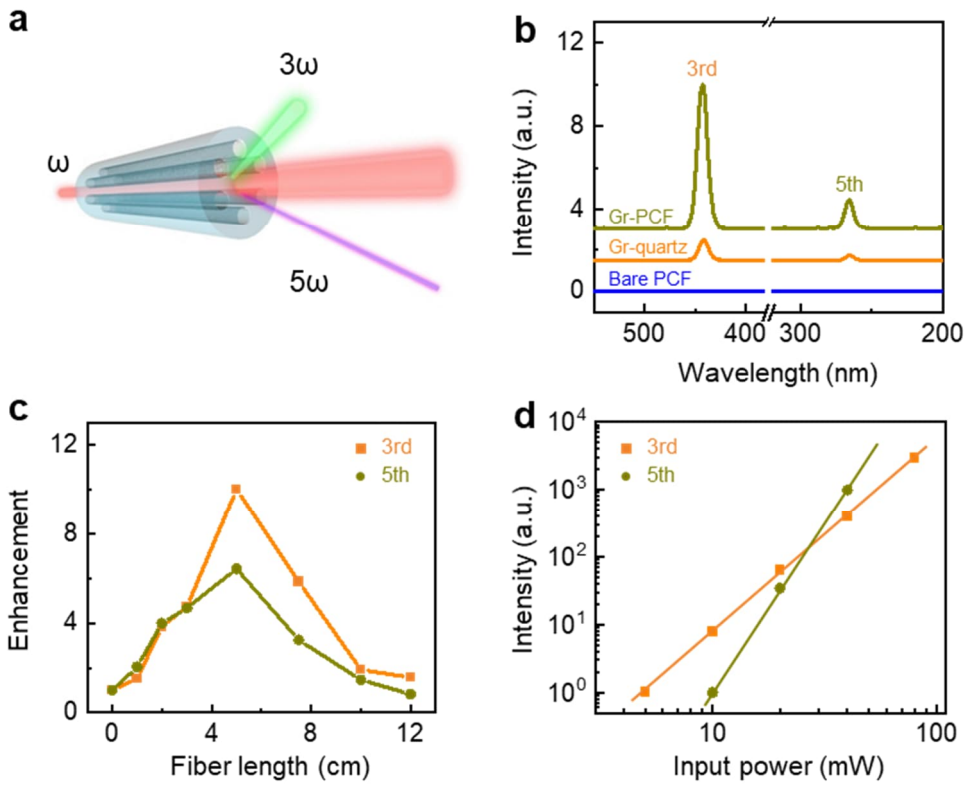

Figure 3. Nonlinear harmonic generation of Gr-PCF. a) Schematic of third and fifth harmonic generations in Gr-PCF. b) Third and fifth harmonic spectra of Gr-PCF, Gr-quartz and bare PCF under the excitation of 1330 nm. The fifth harmonic spectra are magnified by 20 times for clarity. c) Fiber length dependent third and fifth harmonic generation enhancements compared with that on the plane quartz. d) Excitation power dependent third and fifth harmonic intensity of Gr-PCF.

In addition, an all-fiber mode-maintaining mode-locked laser, as a typical demonstration of imaginary-part-related applications, was also demonstrated based on the designed Gr-PCF as a saturable absorber (SA) at the communication band of ~1550 nm (**Figure 4**a). To obtain shorter pulse width and improve the self-starting capability of mode-locked laser, the Gr-PCF SA with the large nonlinear absorption modulation depth is desirable.[33] Here, the modulation depth (α_s) can be defined as the difference in transmittance under the input laser peak intensity (I) of zero and positive infinity according to the fitted function as $T = 1 - \alpha_{ns} - \frac{\alpha_s}{1+I/I_{sat}}$,[9] where T is the transmission, α_{ns} is the non-saturable loss, and I_{sat} is the saturation peak intensity (Figure 4b). By controlling the fiber length and the graphene thickness, the optimal

modulation depth was measured as 6.5% with the acceptable saturable transmission of 22% under the 4 cm-long fiber with quasi-monolayer graphene film (Figure 4c and Figure S9, Supporting Information). Subsequently, a passively mode-locked fiber laser was implemented by dispersion management with a near zero group velocity dispersion (GVD). The maximum output power of the pulsed laser is ~8 mW (under the pump power of 600 mW) with ~4 nm spectral bandwidth, ~1559 nm center wavelength (Figure 4d), ~37 MHz repetition frequency (Figure 4e) and ~2 ps pulse duration (Figure 4f). Besides, the pulse width could be further compressed to ~1 ps for the Fourier transform limited pulse by the GVD compensation outside the cavity, considering the ~4 nm spectral bandwidth.[34]

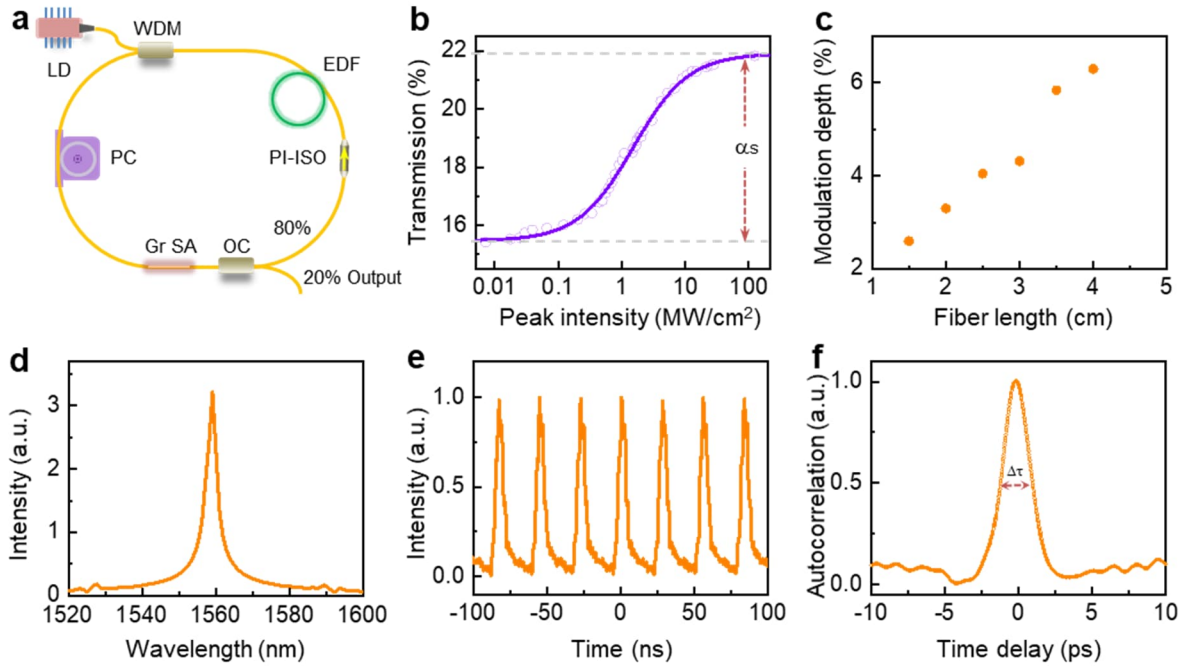

Figure 4. Ultrafast all-fiber laser based on Gr-PCF as saturable absorber. a) Schematic of all-fiber mode-locked laser. b) Transmission measurement of Gr-PCF with a nonlinear absorption modulation depth of 6.5%. c) Length dependent modulation depth of Gr-PCFs. d-f) Spectrum (d), the pulse train (e) and the autocorrelation trace (f) of the output laser. The full-width at half-maximum of the autocorrelation trace (Δτ) is ~2.8 ps, corresponding to a pulse width of ~2 ps, considering the Gaussian convolution factor of 1.414.

In summary, by virtue of the PCCVD method, we successfully synthesized Gr-PCF with controllable thickness and uniform fiber length. Thus, the nonlinear applications, such as

nonlinear harmonic generation and all-fiber mode-locked laser, have been realized with a balance between strong nonlinear light-matter interaction and acceptable linear absorption loss. The excellent nonlinear optical performance and massive manufacturing capacity of the as-fabricated Gr-PCF via the PCCVD strategy demonstrate its distinct superiorities compared with that by transfer techniques. In addition, combined with the well-designed structure of optical fiber, Gr-PCF can be further extended in versatile optical nonlinear applications, such as optical parametric amplification, optical frequency comb and multi-wavelength mode-locked laser.

Experimental Section

Synthesis of Gr-PCFs by PCCVD. The PCFs (~10 μm solid core diameter and ~125 μm fiber diameter, NKT Photonics, LMA-10) were loaded into the center of a one-inch quartz tube within a three-zone high-temperature furnace (Thermo Lindberg/Blue) after removing its outer polymer coating. The CVD chamber was then heated to the desired growth temperature of 1100 ℃ with the rate of 20 ℃/min. For the graphene growth, CH_4 (20 sccm) and H_2 (80 sccm) were introduced to the CVD system for hours. The growth pressure for graphene growth was controlled by a flow valve (MKS 253B) ranging from 0.5 to 20 Torr. After the growth, the as-fabricated Gr-PCFs were naturally cooled down to the room temperature under the mixture gas of hydrogen and argon.

Characterization of Gr-PCFs. Optical images of Gr-PCFs were obtained by a Nikon LV100ND microscope. SEM observations were conducted by FEI Quattro S at 10-20 kV acceleration voltage. EDS was performed by DigiView/Octane Elect. Raman spectra were obtained with LabRAM HR-800 with a 532 nm laser and 100 × objective. AFM was characterized in a Bruker Dimension Icon atomic force microscope to measure graphene thickness on the inner holes of PCFs. HR-TEM characterizations were taken by a FEI Titan Themis G2-300 system with an acceleration voltage of 80 kV. For the Raman, AFM and HR-TEM characterizations, Gr-PCF was immersed into hydrofluoric acid solution (20 wt%) to dissolve silica fiber, followed by transferring collapsed graphene tubes onto silicon substrates or TEM grids.

Fluid simulation. The gas flow velocity and carbon concentration were calculated by finite element method (FEM). The simulated diameter of the fiber hole was set as 2.6 μm. During the simulations, the reactant gas entered through the inlet, while the outgassing wall boundary condition was used for this inlet. To obtain more accurate results, the triangle mesh was also applied to the calculation.

Measurement of the harmonic generation. The excitation laser (1330 nm, 150 fs, 250 KHz) was generated from an optical parameter amplifier (Mira-OPO-9450, Coherent) pumped by high-power Ti-sapphire oscillator (Coherent Vitara-T, Coherent) and focused on the port core of Gr-PCF or graphene on the planar quartz. The third and fifth harmonic signals were collected by an objective lens via a transmission light path to a spectrograph equipped with an ultraviolet to visible charge coupled device (DU420A-BU2, Andor) after filtering the excitation laser.

Characterization of saturable absorption. A pulsed fiber laser (Origami 15, NKT Photonics) with the center wavelength of ~1550 nm, the pulse width of 150 fs, and repetition frequency of 100 MHz, Origami 15, NKT Photonics) was utilized to measure the saturable absorption ability of Gr-PCF. Then, the input laser was divided by 90%/10% through a fiber optics coupler for real-time monitoring the power, where 90% for incident laser and 10% for monitoring. The input fiber (SM-28e+, Corning) was aligned with the Gr-PCF using two sets of microscopies along different direction. By comparing output laser power with the monitoring power, the power-dependence transmission could be measured.

Characterization of all-fiber mode-locked laser based on Gr-PCF. A pump laser (976 nm) was coupled into the ring cavity of the fiber laser by using a wavelength-division multiplex (980 nm/1550 nm), and then pumped the gain medium (the 60-cm-long Er-fiber, Er110 4-125, LIEKKI). The laser in the ring cavity could only propagate along one direction by inserting a polarization-independent isolator. The Gr-PCF was integrated into the fiber ring as a saturable absorber for mode locking and the pulsed laser was outputted via 20% port of the fiber coupler, while the spectrum was optimized by a polarization controller. The total GVD of the fiber ring was 0.0012 ps^2, which was near-zero dispersion, for the dispersion management configuration. The spectrum was measured by a Fourier transform infrared spectrometer (OSA205C, Thorlabs), while the pulse train was monitored via the photodetector (DET08CFC/M, Thorlabs) and the oscilloscope (DS6104, Rigol). The pulse width was obtained by autocorrelation trace measurement via the auto-correlator (Pulsecheck USB 50, APE).

Supporting Information
Supporting Information is available from the Wiley Online Library or from the author.

Acknowledgements:
Y. Cheng, W. T. Yu, J. Xie and R.Y. Wang contributed equally to this work. This work was supported by the Beijing National Laboratory for Molecular Sciences (BNLMS- CXTD-202001), National Key Basic Research Program of China (973) (2016YFA0200103), the National Natural Science Foundation of China (52025023, 51991342, 52021006, 11888101), the Strategic Priority Research Program of Chinese Academy of Sciences (XDB33000000), The Key R&D Program of Guangdong Province (2020B010189001, 2019B010931001 and 2018B030327001), Pearl River Talent Recruitment Program of Guangdong Province (2019ZT08C321), Beijing Natural Science Foundation (JQ19004), Beijing Municipal Science & Technology Commission (Z181100004818003, Z201100008720006), Zhongyuan Thousand Talents Program of Henan Province and National Top-notch Young Talents of Ten Thousand Talents Program.

References:

[1] K. C. Kao, G. A. Hockham, *Proc. Inst. Electr. Eng.* **1966**, *113*, 1151.

[2] J. C. Knight, *Nature* **2003**, *424*, 847.

[3] D. J. Richardson, J. M. Fini, L. E. Nelson, *Nat. Photon.* **2013**, *7*, 354.

[4] L. Thevenaz, *Nat. Photon.* **2008**, *2*, 474.

[5] L. F. Mollenauer, *Science* **2003**, *302*, 996.

[6] D. Skryabin, F. Luan, J. Knight, P. S. J. Russell, *Science* **2003**, *301*, 1705.

[7] J. M. Dudley, G. Genty, S. Coen, *Rev. Mod. Phys.* **2006**, *78*, 1135.

[8] L. Caspani, D. Duchesne, K. Dolgaleva, S. J. Wagner, M. Ferrera, L. Razzari, A. Pasquazi, M. Peccianti, D. J. Moss, J. S. Aitchison, R. Morandotti, *J. Opt. Soc. Am. B* **2011**, *28*, A67.

[9] F. Wang, A. Rozhin, V. Scardaci, Z. Sun, F. Hennrich, I. White, W. I. Milne, A. C. Ferrari, *Nat. Nanotechnol.* **2008**, *3*, 738.

[10] P. J. Sazio, A. Amezcua-Correa, C. E. Finlayson, J. R. Hayes, T. J. Scheidemantel, N. F. Baril, B. R. Jackson, D.-J. Won, F. Zhang, E. R. Margine, *Science* **2006**, *311*, 1583.

[11] A. Abouraddy, M. Bayindir, G. Benoit, S. Hart, K. Kuriki, N. Orf, O. Shapira, F. Sorin, B. Temelkuran, Y. Fink, *Nat. Mater.* **2007**, *6*, 336.

[12] B. J. Eggleton, B. Luther-Davies, K. Richardson, *Nat. Photon.* **2011**, *5*, 141.

[13] J. M. Dudley, J. R. Taylor, *Nat. Photon.* **2009**, *3*, 85.

[14] Y. Li, Y. Rao, K. F. Mak, Y. You, S. Wang, C. R. Dean, T. F. Heinz, *Nano Lett.* **2013**, *13*, 3329.

[15] X. Jiang, N. Y. Joly, M. A. Finger, F. Babic, G. K. Wong, J. C. Travers, P. S. J. Russell, *Nat. Photon.* **2015**, *9*, 133.

[16] N. Yoshikawa, T. Tamaya, K. Tanaka, *Science* **2017**, *356*, 736.

[17] A. Autere, H. Jussila, Y. Dai, Y. Wang, H. Lipsanen, Z. Sun, *Adv. Mater.* **2018**, *30*, 1705963.

[18] K. Chen, X. Zhou, X. Cheng, R. Qiao, Y. Cheng, C. Liu, Y. Xie, W. Yu, F. Yao, Z. Sun, F. Wang, K. Liu, Z. Liu, *Nat. Photon.* **2019**, *13*, 754.

[19] A. Martinez, Z. Sun, *Nat. Photon.* **2013**, *7*, 842.

[20] S. Y. Choi, D. K. Cho, Y. W. Song, K. Oh, K. Kim, F. Rotermund, D. I. Yeom, *Opt. Express* **2012**, *20*, 5652.

[21] Y.-H. Lin, C.-Y. Yang, J.-H. Liou, C.-P. Yu, G.-R. Lin, *Opt. Express* **2013**, *21*, 16763.

[22] Q. Bao, H. Zhang, B. Wang, Z. Ni, C. H. Y. X. Lim, Y. Wang, D. Y. Tang, K. P. Loh, *Nat. Photon.* **2011**, *5*, 411.

[23] W. Li, B. Chen, C. Meng, W. Fang, Y. Xiao, X. Li, Z. Hu, Y. Xu, L. Tong, H. Wang, W. Liu, J. Bao, Y. R. Shen, *Nano Lett.* **2014**, *14*, 955.

[24] E. J. Lee, S. Y. Choi, H. Jeong, N. H. Park, W. Yim, M. H. Kim, J.-K. Park, S. Son, S. Bae, S. J. Kim, K. Lee, Y. H. Ahn, K. J. Ahn, B. H. Hong, J.-Y. Park, F. Rotermund, D.-I. Yeom, *Nat. Commun.* **2015**, *6*, 6851.

[25] G. Li, S. H. Huang, Z. Li, *Phys. Chem. Chem. Phys.* **2015**, *17*, 22832.

[26] S. Bhaviripudi, X. Jia, M. S. Dresselhaus, J. Kong, *Nano Lett.* **2010**, *10*, 4128.

[27] J. H. Cho, S. R. Na, S. Park, D. Akinwande, K. M. Liechti, M. A. Cullinan, *Nanotechnology* **2019**, *30*, 235602.

[28] Q. Liu, Y. Gong, J. S. Wilt, R. Sakidja, J. Wu, *Carbon* **2015**, *93*, 199.

[29] Y. Cheng, K. Wang, Y. Qi, Z. Liu, *Acta Phys. -Chim. Sin.* **2021**, *37*, 2006046.

[30] G. Cui, Y. Cheng, C. Liu, K. Huang, J. Li, P. Wang, X. Duan, K. Chen, K. Liu, Z. Liu, *ACS Nano* **2020**, *14*, 5938.

[31] X. D. Chen, Z. Chen, W. S. Jiang, C. Zhang, J. Sun, H. Wang, W. Xin, L. Lin, M. K. Priydarshi, H. Yang, Z. B. Liu, J. G. Tian, Y. Zhang, Y. Zhang, Z. Liu, *Adv. Mater.* **2017**, *29*, 1603428.

[32] H. Wang, X. Xu, J. Li, L. Lin, L. Sun, X. Sun, S. Zhao, C. Tan, C. Chen, W. Dang, H. Ren, J. Zhang, B. Deng, A. L. Koh, L. Liao, N. Kang, Y. Chen, H. Xu, F. Ding, K. Liu, H. Peng, Z. Liu, *Adv. Mater.* **2016**, *28*, 8968.

[33] H. H. Liu, K. K. Chow, *Opt. Lett.* **2014**, *39*, 150.

[34] C. Lefort, T. Mansuryan, F. Louradour, A. Barthelemy, *Opt. Lett.* **2011**, *36*, 292.